Reshaping covalent nanowires by exploiting an unexpected plasticity mediated by deformation twinning

Sergei Vlassov[*1], Sven Oras[2], Annamarija Trausa[3], Tauno Tiirats[2], Edgars Butanovs[2,3], Boris Polyakov[3], Veronika Zadin[2] and Andreas Kyritsakis*[*2]*

1) *Institute of Physics, University of Tartu, W. Ostwaldi 1, 50411 Tartu, Estonia*
2) *Institute of Technology, University of Tartu, Nooruse 1, 50411 Tartu, Estonia*
3) *Institute of Solid State Physics, University of Latvia, LV-1063 Riga, Latvia*

**Corresponding author. e-mail: sergei.vlassov@ut.ee, andreas.kyritsakis@ut.ee*

Keywords: CuO, kinking, twinning, nanowires, nanomanipulation, molecular dynamics, plastic deformation

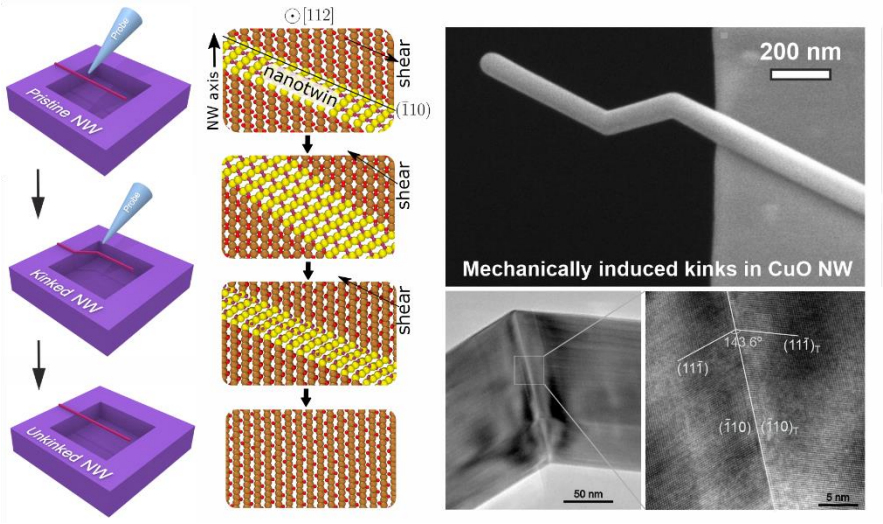

Abstract

Nanowires are among the most studied nanostructures as they have numerous promising applications thanks to their various unique properties. Furthermore, the properties of nanowires can be tailored during synthesis by introducing structural defects like nano-twins, periodic polytypes, and kinks, i.e., abrupt changes in their axial direction. Here we report for the first time the post-synthesis formation of such defects, achieved by exploiting a peculiar plasticity that may occur in nano-sized covalent materials. Specifically, we find that single-crystal CuO nanowires can form double kinks when subjected to external mechanical loading. Both our microscopy and atomistic modeling suggest that deformation-induced twinning along the $(\bar{1}10)$ plane is the mechanism behind this effect. Finally, we provide experimental and computational evidence that the reverse process, i.e., un-kinking, is achievable as well. The phenomenon reported here provides novel insights into the mechanisms of plastic deformation in covalent nanowires and offers potential avenues for developing techniques to customize the shape of nanowires post-synthesis and introduce new functionalities.

1. Introduction

In recent years, mechanical tests on small volume covalent materials (nanospheres, nanowires, and nanopillars) reveal many unique and intriguing mechanical properties which were never observed in their bulk counterparts [1–3]. For instance, Östlund et. al. [4] observed the ductility of micromachined silicon (Si) pillars comparable to that of metals in a room-temperature compression tests, when the size of the Si sample was reduced below 300 nm. Wu et. al. [5] reported a brittle to plastic transition during compressive deformation at room temperature for monoclinic beta-phase gallium oxide (β-Ga_2O_3) single crystals with reduction of the pillar size below 800 nm. Mignerot et al [6] observed plastic deformation of InSb micron-sized pillars during micro-compression tests at room temperature and found stress-induced nano-twin formation.

To further decrease the size of a specimen, a convenient alternative to micromachining is a direct synthesis of nanostructures, especially in the form of nanowires (NWs). Being nanoscale in two dimensions, NWs still exhibit significantly different characteristics in comparison to their 3D counterparts. At the same time, the 1D geometry facilitates the characterization and manipulation of such structures providing more flexibility in the conduction of experiments with individual objects in comparison to nanoparticles (0D) [7].

Single crystal NWs can be synthesized relatively easily in a wide range of lengths and diameters. For instance, CuO NWs can be grown by just annealing a copper foil in air at several hundred degrees Celsius [8]. Their mechanical properties have been found to be purely elastic up to a critical strain, followed by brittle fracture when the latter is exceeded [9,10]. The ultimate strength was comparable to the theoretical strength of CuO, indicating that thermal growth yields single-crystalline NWs with low concentration of critical defects. Yet, more exotic mechanical properties were found by Sheng et al [11], who demonstrated anelasticity of axially twinned CuO NWs during bending tests inside a transmission electron microscope (TEM), attributing it to the cooperative motion of twin-associated atoms.

In general, the properties and functionalities of NWs can be modified by introducing various defects like dopants [12,13], oxygen vacancies [14], nano-twins [6,15], and kinks [16], i.e. abrupt changes in the growth direction of a NW. In particular, kinked NWs are attracting an increasingly growing attention, driven by their potential use as building blocks in electronic [17–19] and nanomechanical devices [20,21], as well as their reportedly enhanced mechanical durability [22]. State of the art synthesis protocols of semiconductor NWs provide rather good control over the location and number of kinks, by modifying the growth conditions (temperature, gas pressure and composition) during their growth [16].

In the present study, we report a completely different approach to NW kinking, which can open novel pathways for the deeper understanding of the unique mechanical properties of nanostructures, as well as their potential exploitation. We achieve kinking post-synthesis, by the mechanical manipulation of initially straight thermally grown CuO NWs. To the best of our knowledge, mechanically induced post-synthesis kinking of covalent NWs is observed for the first time. We describe three different manipulation scenarios that lead to post-synthesis kinking. Moreover, we demonstrate that kinking can be reversible. Our experiments are supported by molecular dynamics simulations and explained by a mechanism of deformation-induced crystal twinning.

2. Results

2.1. Sample preparation

We grew CuO NWs by annealing a copper foil, as described in Ref. [23]. We inspected the as-grown CuO NWs on their original growth substrate (Cu foil) using scanning electron microscopy (SEM). All NWs were straight and without kinking. Their length reached up to 5-10 µm, with diameters in the range of 50-200 nm. The NW cross-sections had an irregular shape, characteristic to monoclinic crystal systems. These NW parameters are in good agreement with the ones previously reported in the literature on thermally grown CuO NWs [8,23,24]. Detailed microscopy images of the as-grown NWs can be found in the Supporting Information (Figures S1-2).

The NWs were then transferred mechanically on three different types of Si substrates, by manually pressing and then shearing the Cu foil with the NWs against the substrates (see Figure 1a). Type I substrates were unetched Si wafers, where the NWs lied on their flat surface. Type II substrates had square-shaped etch pits with a side length in the order of few µm and depth in the order of several hundreds of nm. Finally, substrates of type III had 3 µm wide parallel trenches separated by 900 nm wide planes of un-etched Si. The slope of the sidewalls of the pits and trenches relative to the main surface of the silicon is 54.7 degrees, which corresponds to the angle between the (111) and (001) planes in Si. As a result, some NWs were partially protruding above the etch pits and trenches of the type-II and III Si substrates (see Figure 1b,c).

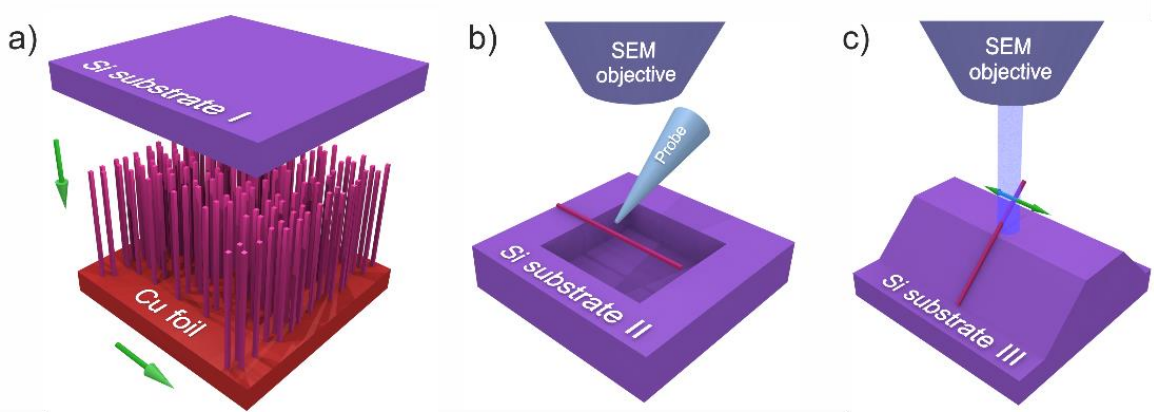

Figure 1: Schematic representation of the sample substrates we used, the positioning of the CuO nanowires on them, and the manipulation operations that induced kinking.

2.2. Kinking by mechanical transfer

Upon examining the CuO NWs that were mechanically transferred onto the Si sample substrates or the Si TEM grid as depicted in Figure 1a, we found that a significant fraction of them appeared to have deformations that looked like so-called “kinks”, i.e., they had an abrupt change in orientation without losing their structural integrity. Considering that no kinked NWs were observed in the original growth substrate, we can conclude that this transformation occurred during mechanical transfer. The kinking angles of our CuO NWs appeared to be within a very narrow range (see Figure 2a - inset), with a median value of 143.2 ± 2.9 degrees. The latter was measured after analyzing the SEM images of fifty kinked NWs on the type-I (flat) sample substrate, as shown Figure 2a. This angle uniformity indicates that the observed deformation is directly related to the structure of the CuO crystal, rather than being a random defect. Moreover, with a very few exceptions, which can be probably attributed to post-kinking fracture, the kinked NWs always had a double kink that divided the NW into three segments, as seen in Figure 2. Finally, in a few cases, we observed NWs with multiple double kinks (see Figure S3d).

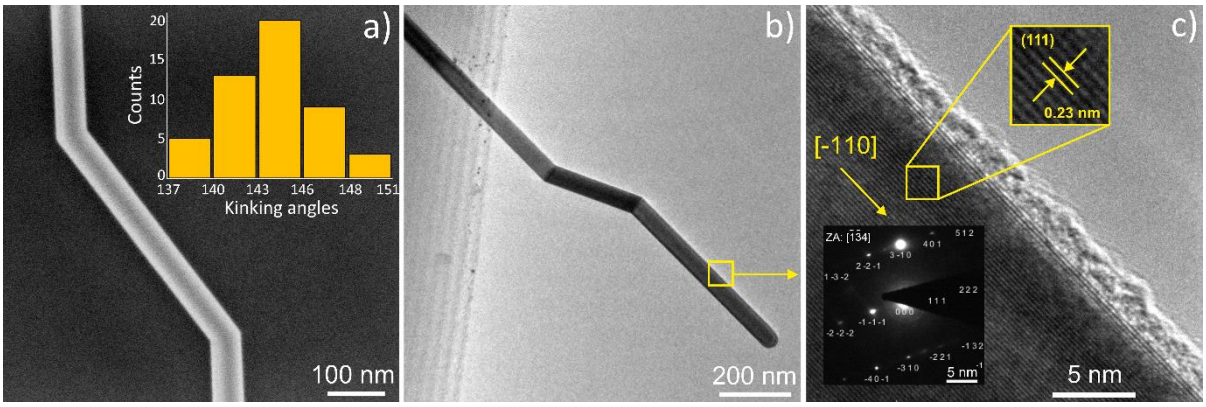

Figure 2. (a): SEM image of a CuO NW kinked after mechanical transfer on a flat Si wafer. The inset shows a histogram of the kinking angles measured over 50 kinked NWs from the SEM images. (b): TEM image of a CuO NW kinked after mechanical transfer on the Si TEM grid. (c): TEM image of the same NW at higher magnification and corresponding SAED image. NW growth direction [-110] is indicated by an arrow.

2.3. Nanomanipulation-induced kinking and unkinking

We then performed a series of nanomanipulation tests on partially suspended CuO NWs transferred to structured Si wafer (Substrate type II), to explore their behavior under external mechanical loading. The NWs were pushed by a tungsten probe attached to a nanomanipulator (Figure 1b). We conducted the experiments inside SEM, which provided real-time visual feedback. The movement of the nanomanipulator used in the experiment is either smooth within the "scan mode" of the piezo scanner, which has a limited range of a few microns, or coarse (abrupt) within the "step mode", based on the stick-slip motion of the piezoelectric actuator (more details in section III of the SI). This abrupt movement results in the excitation of fast-decaying oscillations in the manipulator-probe system with an amplitude in the order of several µm. We found that a coarse movement of the probe can induce kinking in CuO NWs that are protruding over the etch pit of the Si sample substrate. The timescale of kinking event lies below the temporal resolution of the SEM (scanning rate); thus, we were able to see only images before and after it.

Figure 3a-e illustrates the sequence of mechanical nanomanipulations aimed to produce kinking in a single CuO NW (frames taken from Video 1, available in the SI). The CuO NW is partially suspended over the etch pit of the Si sample substrate (darker area is the bottom of the pit). The probe of the nanomanipulator is first placed near the NW. Then it pushed the NW against the sidewalls of the pit. At a certain moment (Figure 3c), the manipulator makes a coarse movement ("step") that results in the kinking of the NW. In most cases where such a kinking was achieved, the kinked region was in close proximity to the sharp edge of the pit or near the corner of the pit. In total, twenty-three kinking events were recorded during nanomanipulation experiments. However, brittle fracture of NWs was a more frequent result of "step mode" manipulation.

No kinking was achieved by manipulation in the scan mode of the nanomanipulator. This indicates that mechanically induced kinking requires specific conditions to be fulfilled. During bending in scan mode, the NWs remained fully elastic until the ultimate strength limit that resulted in brittle fracture was reached. Quantitative measurements of the bending strength of these NWs were performed in our previous study [9] and high values of 8.2 ± 2.7GPa were found, which is indicative of a pristine single crystal with low concentration of critical defects. This agrees with the structural analysis presented in the corresponding section.

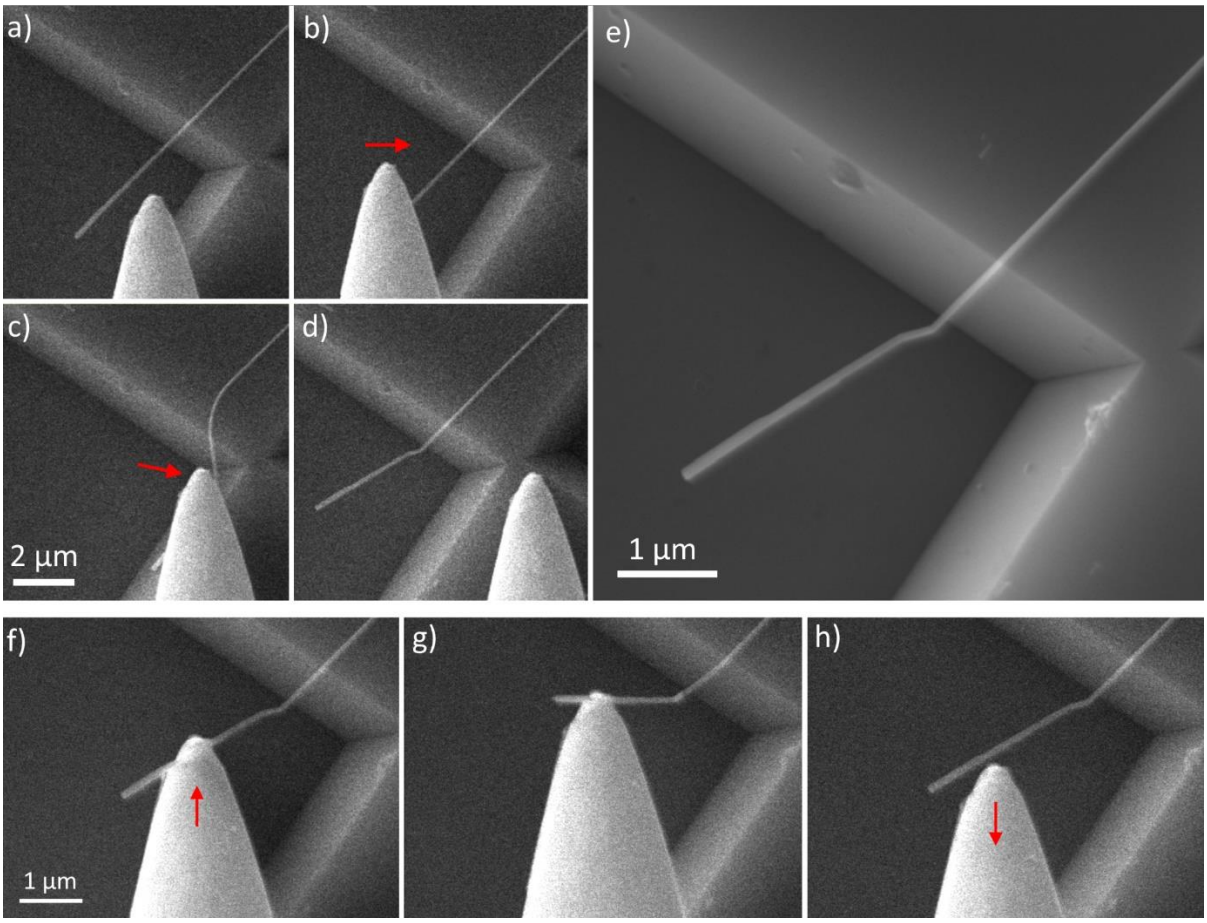

Figure 3. Nanomanipulation-induced kinking in CuO NW that is protruding over the etch pit in Si sample substrate. a) Initial configuration of CuO NW partially suspended over the pit in Si sample substrate (darker area is the bottom of the pit). b) The probe of the nanomanipulator is placed above the NW and starts moving down and to the right. c) The probe pushes the NW against the sidewalls of the pit. Nanomanipulator moves in scan mode followed by coarse movement that results in kinking of CuO NW. d) and e) Results of the nanomanipulations. f-h) Nanomanipulation of the same previously kinked CuO NW, observing its behaviour under external load.

By pushing the already kinked NWs, we found that they are rather durable and behave elastically, preserving the angle of the kink in the absence of an external force. At severe deformations or as a result of a coarse movement of the manipulator, the NWs can break at the kink. However, in most cases fracture occurs at arbitrary locations outside the kinked region, indicating that there is no significant weakening of the crystal at the kink. Chosen frames from a single nanomanipulation experiment carried out on a previously kinked CuO NW are shown in Figure 3f-h (see also Video 2 in SI). This is the same NW that was kinked in Figure 3f-h. The probe of the nanomanipulator moves under the CuO NW (Figure 3f) and then slowly pushes it to the side and upwards (Figure 3b). When the probe is retracted, the NW immediately restores its shape without any additional deformation (Figure 3c). The kink location and kinking angles are preserved.

In a single case, we were able to first kink and then unkink a single CuO NW back to its initial straight profile (Figure 4 and Video 3 in the SI). The probe was placed in close proximity above the NW and then moved by a coarse nanomanipulator motion (Figure 4b). When the probe was retracted, the NW appeared to be kinked (Figure 4c,d). Next, the kinked NW was pushed and displaced by the probe (Figure 4e,f) in an attempt to see if it will break at the kink. Instead, when the probe was retracted, the NW appeared to be not only intact, but also unkinked (Figure 4g,h). This unkinking seems to require even more specific conditions to occur in comparison to kinking, as we did not succeed to repeat it

with other NWs. It seems that an important factor is that a sufficiently long NW is suspended over the pit and remains suspended.

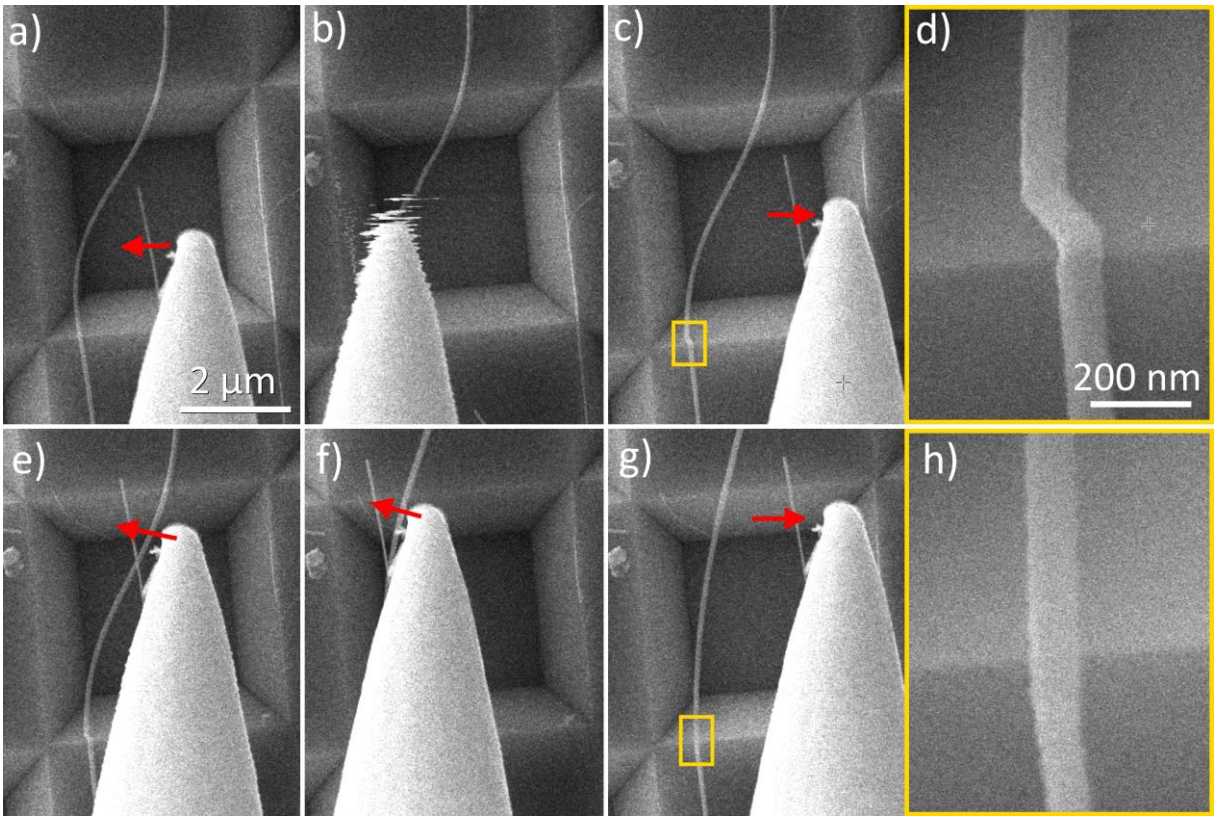

Figure 4. Chosen frames of kinking and unkinking of a single CuO NW by means of nanomanipulation.

2.4. Kinking by electron-beam-induced oscillation

We found that kinking of CuO NWs can be achieved also by electron-beam induced oscillations of the free-standing part of a NW. This phenomenon was observed for NWs transferred to the type-III patterned Si sample substrate (see Figure 1b). It happened at slow e-beam scanning speed, which caused auto oscillations in protruding part of NW. One such case is shown in Figure 5. First, at the expense of image quality, the NW is imaged at a high scan rate (few frames per second) so that the electron flux is not enough to induce oscillations (Figure 5a). Then we imaged the NW at a slow scanning speed that leads to NW self-oscillations. These oscillations can be noted by the NW part above the red arrow that appears smeared in Figure 3b, as the SEM imaging is generated by scanning the e-beam line by line (horizontally) starting from the top left corner towards the bottom right corner.

When the beam has reached the point indicated by the red arrow in Figure 5b, the oscillating part jumps into contact with the substrate. Therefore, Figure 5b contains partial data from two states of the NW in one image. The upper part above the red arrow corresponds to an oscillating NW, while lower part shows the NW resting in contact with the top plane of the Si structure. By this moment, a kinking event had already happened. The result of the oscillation-induced kinking is shown at different magnifications in Figure 5c,d.

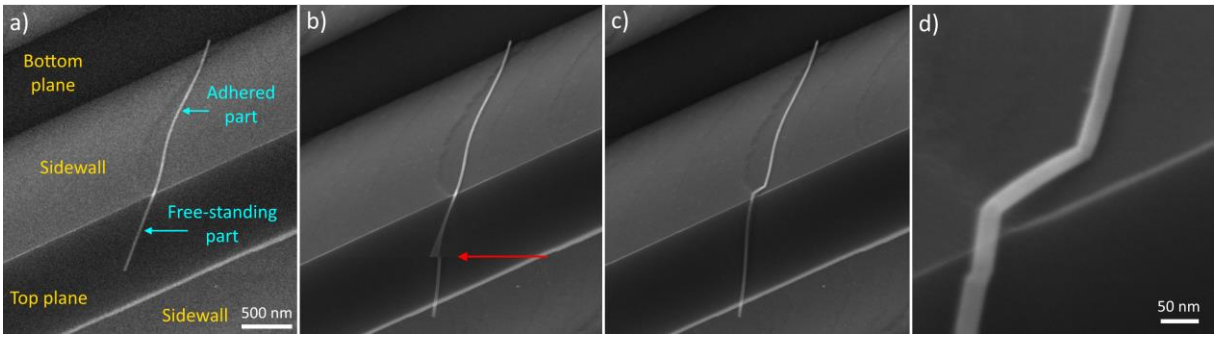

Figure 5. Electron-beam-induced oscillation followed by kinking of the CuO NW on the structured Si substrate. The accelerating voltage of the e-beam is 10kV.

Such a kinking event initiated by e-beam-induced oscillations occurred very rarely (few cases per thousands of observed CuO NWs that were protruding above the substrate). Finally, in a few even rarer cases (three cases out of a few hundred experiments where considerable NW oscillations were observed), the e-beam-induced oscillations resulted in what looks like melting of CuO NWs. The oscillating part of the NW abruptly turned into a sphere (see Figure S5). More details and corresponding discussion can be found in the Supportive Information file.

2.5. Structural characterization of kinked CuO NWs

To understand the kinking mechanism, we first need to investigate the exact crystallographic structure of the NWs at the kink area. For this purpose, we performed high-resolution TEM imaging of several kinked CuO NWs. Figure 6a gives such a TEM image of a kinked NW at exactly the kinked area. In Figure 6b, we zoom closer at the kink to observe its exact crystallographic structure. Figure 6c gives the corresponding SAED image of the same kink region. The following paragraphs give an exact analysis of these images that reveals the crystallographic structure of the CuO NW at the kink.

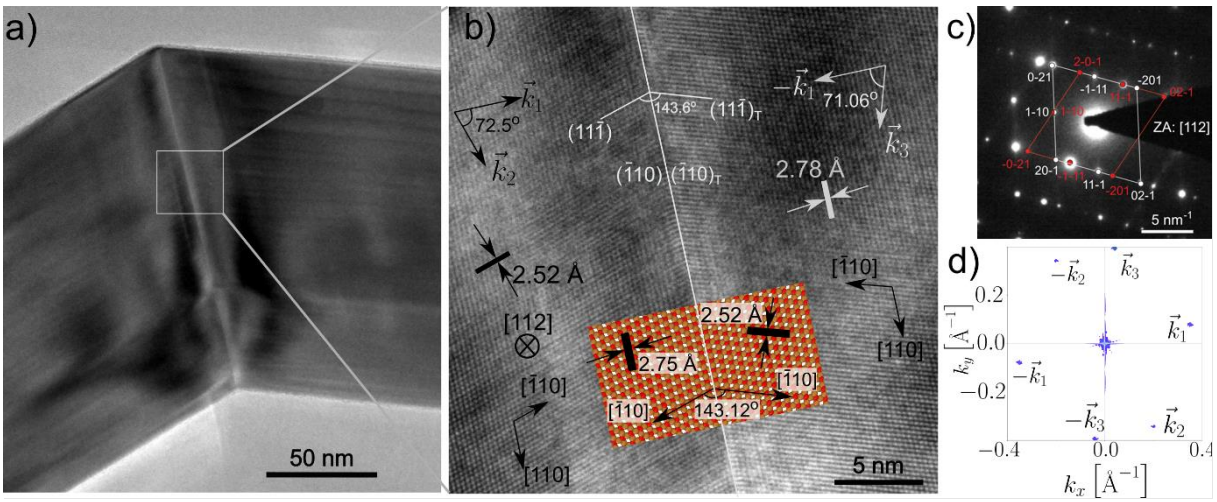

Figure 6: a) TEM image of the kinked area of the CuO NW. b) High resolution TEM image of the area designated in (a). The inset shows an atomistic model of the CuO twin boundary. The crystallographic planes are shown with white lines and the projections of crystallographic directions on the image with arrows. The inter-place distances found by the Fourier analysis of the image are shown on the TEM image, while the theoretical ones are shown in the MD model inset. White and black fonts have been used to ensure maximum visibility in each case. c) SAED image of the same kink region, showing excellent agreement with the zone axis of the image being [112]. The SAED image combines reflexes from the left and right part of NW (before and after kink), the white and red rhombi indicate corresponding sets of reflexes. In the SI file expanded version of the kink SAED can be found [Fig.S4]. d) Fourier transform of the TEM image, with the six peaks at the corresponding wavenumbers $\pm\vec{k}_{1,2,3}$ *indicated.*

CuO forms a monoclinic crystal system of the C2/c space group (No 15), with the following lattice parameters at room temperature (T=293.3 K) [25] a=4.6855 Å, b=3.4237 Å, c=5.1302 Å, β=99.545°. Figure 6b indicates strongly that the kink is formed by a twin boundary (shown with a white line). To investigate its exact crystallographic structure deeper, we start with the hypothesis that the twinning plane is the $(\bar{1}10)$, i.e., parallel to $[110], [112]$, and $[001]$, and the growth direction is $[\bar{1}10]$, as indicated in Figure 6b. We shall now analyse the images to confirm this.

Table 1: Fourier transform peaks and the corresponding crystallographic planes.

Vector	$\vec{k}_1$	$\vec{k}_2$	$\vec{k}_3$
$k_x(\text{Å}^{-1})$	0.351	0.202	0.04
$k_y(\text{Å}^{-1})$	0.082	-0.341	0.395
$\lvert k\rvert(\text{Å}^{-1})$	0.360	0.340	0.397
$\lvert k\rvert^{-1}(\text{Å})$	**2.776**	**2.521**	**2.517**
Angle with $\vec{k}_1$	0	**72.52°**	**71.07°**
Corresponding crystal plane	$(\bar{1}10)$	$(11\bar{1})$	$(11\bar{1})_T$
Inter-plane distance	**2.751**	**2.524**	**2.524**
Angle with $(\bar{1}10)$	0	**71.56°**	**71.56°**

We start by observing that the SAED image gives an excellent agreement with the zone axis of the image being $[112]$. To precisely quantify the crystallographic structure features of the TEM image, we analysed its periodicities by two-dimensional Fourier analysis. The resulting spectrum (absolute part) is shown in Figure 6d. We clearly see that the Fourier image exhibits three very sharp peaks (and their negatives), the location of which are summarized in Table 1, along with the data of the corresponding crystal planes. Both the magnitudes and the angles of these vectors are perfectly consistent with our hypothesis, as they match excellently with the inter-plane distances and angles of the $(\bar{1}10)$ and $(11\bar{1})$ planes, shown in bold in Table 1, as well as the spots of the SAED image (see Figure 1c). The directions of these vectors are also indicated on Figure 6b along with the corresponding wavelengths and angles. We note that neither the $[\bar{1}10]$, nor the $[110]$ directions are parallel to the image plane, meaning that the arrows in the image indicate their projections on it. In fact, $[\bar{1}10]$ and $[110]$ form 2.01^o and 23.52^o angles with the image plane, correspondingly.

The full kink angle predicted theoretically by our hypothesis, i.e., two times the angle between the direction $[\bar{1}10]$ and the plane $(\bar{1}10)$ is 142.9^o, with its projection on the image plane being slightly higher at 143.12^o. These values are in excellent agreement with the corresponding value extracted from the Fourier analysis of the TEM image 143.6^o, as well as with the average kinking angle $143.2^o \pm 2.9^o$ found upon measuring many kinked NWs using SEM. Hence, our hypothesis on the crystallographic structure of the kink is confirmed by the experimental data.

2.6. Molecular Dynamics modelling

In order to understand the dynamics of the kinking and the unkinking process shown in Figure 4(e-h), we simulated an infinite CuO crystal where we introduced a nano-twinned band of 4 monoatomic Cu layers, with the twin plane being the $(\bar{1}10)$, as shown in the inset (a) of Figure 7. Our simulations show that under application of shear loading (imposed strain) towards the projection of the growth direction $[\bar{1}10]$ on the twin plane $(\bar{1}10)$ (see the schematics above Figure 7, the twinned band grows, as the twin planes shift layer by layer. Then, upon application of shear strain in the opposite direction, the

twin band shrinks, as it undergoes the exact opposite shift of the twin planes. Finally, after its size shrinks down to a total of six layers, the crystal un-twins upon continuation of the shear loading.

Figure 7 shows the evolution of the total applied shear strain (green, right axis), and the corresponding stress (blue, left axis). A zero-pressure barostat was applied to all the other components of the stress tensor. The sequence of straining and relaxing are shown schematically above the diagram. The plane of deformation (image plane of the schematics) is the one defined by the $[\bar{1}10]$ vector and the normal vector of $(\bar{1}10)$. The insets (a-d) show four snapshots of the atomic system, as seen from the $[112]$ zone axis, with the important directions and planes designated on inset (a). Note that both $[\bar{1}10]$ and its projection to $(\bar{1}10)$ (shear direction) are not exactly parallel to the image plane of the insets; thus, the corresponding arrows show projections to the image plane. The atoms within the twinned band are designated with distinct colors than the bulk of the crystal. The full evolution of this system can be seen in Video 4 attached in the SI.

When we apply a positive strain, (positive direction convention designated in inset (a)), the twinned band grows by four Cu layers, as the upper twin plane shifts three layers upwards and the lower twin plane shifts one layer downwards. The plastic deformation corresponding to these shifts is visible as abrupt drops on the shear stress at t =10.5, 12, 15.1, and 16.8 ps. Then we allow the system to relax with a zero-pressure barostat until $t = 42.55$ ps, which leaves the atomic system in the deformed state depicted in inset (b), i.e., with the twinned band larger than the initial.

After this, we start enforcing a shear strain in the opposite direction, which results in the negative shear stress shown in the figure. At about $t = 50.1$ ps, a small stress release occurs as the system undergoes a shear deformation (simple shear), with the plane of deformation being the $(\bar{1}10)$ i.e., perpendicular to the plane of deformation of the imposed shear (see sec. IVA of the SI for details). As we keep straining, more stress builds up, which is then released by a series of shifts of the twin planes that shrink the twin band, accompanied by a few $(\bar{1}10)$ plane slips. These series of plastic deformations are visible as oscillations on the stress curve, leaving the crystal on the state seen in inset (c), at $t = 75$ ps. Finally, right after (c), a series of atomic rearrangements occurs that completely removes the twin band, leaving behind an almost pristine crystal. We then relax the system to zero pressure, arriving in the final state shown in inset (d), which corresponds to a defect-less CuO crystal.

The above results show that this kind of shear stress, which are most probably obliquitous when a NW undergoes abrupt mechanical deformations (e.g., due to oscillations), can lead to both the growth of a kinked (twinned) band defect, as well as its shrinking and final annihilation. Furthermore, in sec. IVA of the SI, we present in detail an additional simulation of a system with a large, twinned band (large enough that its size does not affect the twin formation energy), where we analyse in detail the atomic layer gliding mechanism that shifts the twin plane upon shear loading. Finally, in sec. IVB of the SI, we present an additional simulation result that shows a possible mechanism that could initiate a small, twinned band from a pristine crystal, upon application of very high shear strain.

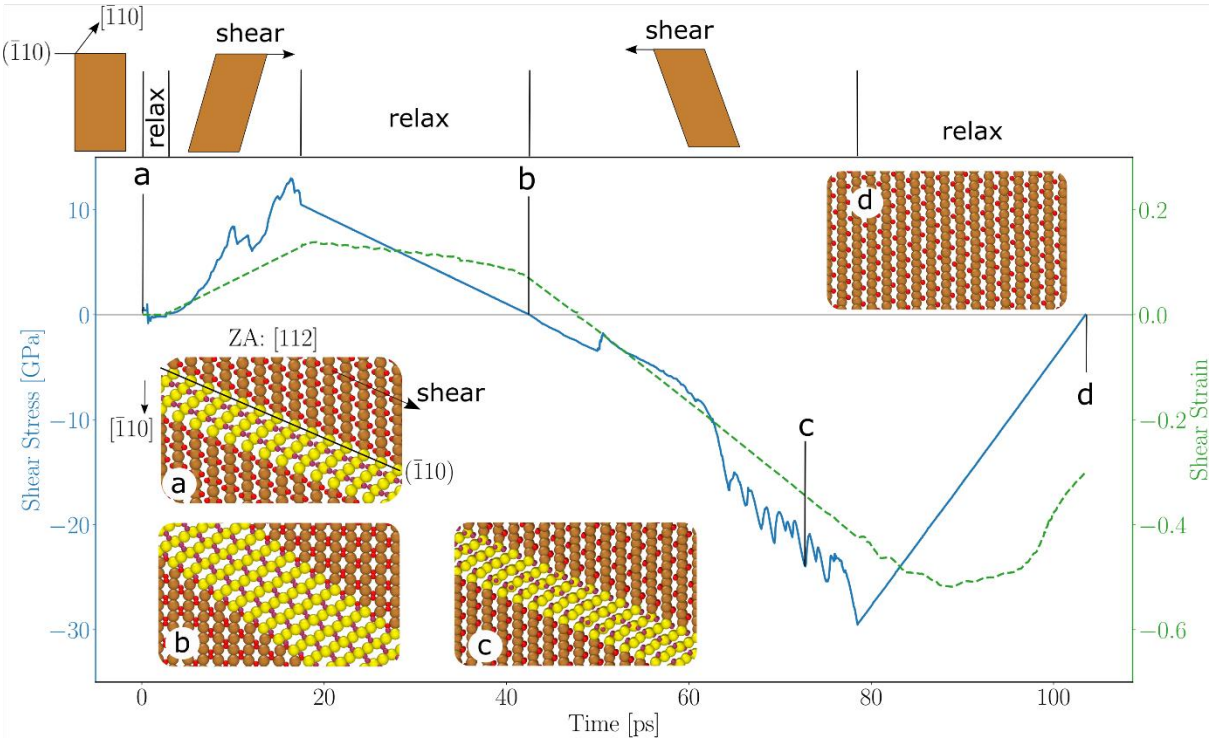

Figure 7: Shear stress and strain evolution of the simulated CuO crystal. The operation simulated at each time interval is represented schematically above each simulation interval, with the image plane of the schematics (plane of deformation) being the one that is parallel to $[\bar{1}10]$ *and perpendicular to* $(\bar{1}10)$*. The four insets give snapshots of the atomistic system as seen from the* $[112]$ *axis, i.e., with the image plane being nearly (but not exactly) parallel to the plane of deformation designated by the schematics the plot. The following instances are shown: (a) initial system, (b) relaxed after positive straining, (c) right before un-twinning, (d) final un-twinned. The atoms within the twinned band are designated in yellow for clarity.*

3. Discussion

Kinking in semiconductor NWs often appears during growth and is a well-known and widely studied phenomenon [16]. However, in our case, the "kinking" was induced post-synthesis in initially straight NWs under completely different experimental conditions: during mechanical transfer of many free-standing NWs from one substrate to another, during oscillations caused by in-situ e-beam irradiation, and during in-situ mechanical nanomanipulation of partially suspended NWs. In all these cases the same plastic deformation (double kinking with angle of approx. 143°) was observed. The nanomanipulation and e-beam induced kinking is relatively hard to reproduce consistently. In the former case, the process is driven by the coarse motion of the nanomanipulator and in the latter by momentum and charge transfer from the beam to the NW. In neither of these cases the mechanical loading is well controllable. Moreover, the adhered NWs have a number of varying parameters, (different lengths of adhered and protruding parts, different diameters, cross-sections, etc.) that may play a significant role in the outcome of manipulation experiments. Hence, we should rely on coincidence of the favourable parameters to induce kinking in individually manipulated NWs. However, in the mechanical transfer scenario, the massive number of NWs that receive various kinds of loading allows for a substantial number of them becoming kinked. Furthermore, the observation of kinking during transfer allows us to rule out the possibility that the e-beam plays an essential role in the kinking process.

There are certain common factors between kinking induced by nanomanipulations and e-beam. In both scenarios NWs were partially suspended and oscillations were observed before kinking. We were unable to induce kinking during either a smooth nanomanipulation operation, nor under e-beam without the specific etched Si substrate that allowed the suspension of NWs under certain angle.

Additionally, the MD simulations showed that the shear loading necessary to induce growth of the kinked band is quite specific in direction. This agrees with the low reproducibility of the nanomanipulation and e-beam induced kinking, suggesting that oscillations may play an important role at least in the in-situ kinking of individual NWs. After making an abrupt motion, the manipulator probe and the NW oscillate in a complex manner, similarly to the case observed under e-beam, resulting in mechanical loading towards many different directions. One of those directions may be favourable for inducing the necessary atomic rearrangements that lead to kinking. Furthermore, kinking mostly appeared when the protruding part of a NW contacted the surface of the Si substrate during nanomanipulations or e-beam induced oscillations. This might be another contributing factor, as NW-substrate adhesion may increase the internal shear loading by fixing the NW ends. Lastly, both shear loading in mechanical transfer and oscillations related to manipulations of NWs may involve triboheat-related temperature rise that might be another contributing factor in the probability of kink formation.

Given the above, we can conclude that in all three experimental scenarios, there is a common underlying plastic deformation mechanism behind the kinking, which can also be reversible under specific conditions. The structural analysis with TEM and SAED images along with the MD simulation results corroborate that this mechanism is deformation induced twinning. Although deformation twinning is quite ubiquitous in metallic materials and alloys [26], such a reversible plasticity is unexpected in covalent nanomaterials, which typically tend to switch from elasticity to fracture [2]. However, the extremely low size that allows for almost defect-less crystal structures within the NWs, has been considered to allow much higher stresses and strains without fracture [2], resulting in the possibility for reversible plasticity, such as the one reported for GaAs NWs [27] and attributed to dislocation activity.

Further research is necessary to study the exact conditions at which the kink is introduced. Quantitative measurements of the kink strength and the forces involved in kinking/unkinking events in a more rigid and controllable force-exertion system should be a subject of a separate study. Furthermore, it is necessary to conduct further atomistic studies to give a deeper understanding of the atomic mechanisms that lead to the twinning. For that purpose, a more accurate potential (force field) for CuO than the COMB3 used here will be necessary. Although the latter is not very accurate (e.g., it predicts the lattice parameters of CuO with an error about 8% compared to experimental values), it qualitatively reproduced the deformation twinning mechanism in very good agreement with the experiments, at least at the extremely low temperature of 1K. However, for deeper quantitative analysis of the mechanism and the investigation of thermal oscillation effects, probably more advanced and accurate Machine-Learning based potentials for CuO will be necessary. Finally, the role of the NW temperature in the kink formation is still an open question, which needs to be investigated by both experiment and simulation.

Deformation twinning and its role in the plastic behaviour of metal nanowires has been thoroughly investigated in tensile and bending tests both experimentally and theoretically for different nanowire materials like Au, Ag, Al, etc. [28–33]. This is the first demonstration of reversible plastic deformation possibility of covalent NWs driven by deformation twinning, observed in experiment and simulated by MD. This opens a new research direction towards understanding quantitatively and exploring exploitation techniques for this NW behaviour, as a deeper understanding of these phenomena shall open a new route for post-synthesis modifications of covalent material single crystals. Finally, the possibility of mechanically induced kinking should be explored for other NW materials as well, as it may enhance their properties and allow for novel functionalities.

4. Conclusions

We have experimentally demonstrated the mechanically induced kinking of CuO NWs. Structural analysis of the kinked NWs with HRTEM and SAED, along with analysis of the kinking angles showed that the kinking corresponds to twinning on the $(\bar{1}10)$ crystal plane of CuO. We propose that this twinning is caused by mechanical deformation in specific direction, occurring during intense oscillations or mechanical transfer of the NWs. Our hypothesis is supported by MD simulations which show that a twin plane can reversibly shift upon application of shear loading along the projection of the $[\bar{1}10]$ direction on the $(\bar{1}10)$ plane. This allows either the growth or shrinking of a twinned crystal band depending on the direction of the shear loading. The newly discovered phenomenon opens a new route for post-synthesis modifications of covalent material single crystals.

5. Methods

5.1. Sample preparation and characterization

CuO NWs were grown by annealing a copper foil at 400 °C for 2h at ambient atmosphere, following the methodology of Ref. [23]. The initial morphological analysis of the as-grown CuO NWs on the original substrate was performed by scanning electron microscopy SEM (Helios NanoLab 600). SiO_2/Si(100) wafers (Semiconductor Wafer, Inc.) with 50 nm thermal oxide were used as substrates for conducting further experiments with individual NWs. The patterned silicon substrates of type II and III were prepared by chemical etching of SiO_2/Si(100) as described in [34]. The crystalline structure of CuO NWs was studied using transmission electron microscopy (TEM, Tecnai GF20, FEI) operated at the accelerating voltage of 200 kV. The selected area electron diffraction (SAED) pattern was processed by CrysTBox software.[35]

5.2. Manipulation of individual nanowires.

We performed two types of manipulations of individual CuO NWs:

- In the first scheme (see Figure 1b), partially suspended CuO NWs were mechanically manipulated on a type-II sample substrate by pushing the suspended end of the NW with a sharp tungsten probe attached to a micromanipulator (Kleindiek MM3A-EM). Experiments were conducted inside SEM (Tescan Lyra XM). The adhesion between the CuO NWs and Si was high enough to hold the adhered part of the NW during manipulation without the need of additional fastening.
- In the second scheme (see Figure 1c), the intense oscillations in partially protruding CuO NWs were induced by the incident electron beam (e-beam) on a type-III sample substrate, inside a SEM (Helios NanoLab 600).

5.3. Simulations

Molecular Dynamics (MD) simulations were ran using the LAMMPS [36,37] MD simulation package. We employed the third version of the Charge Optimized Many-Body potential (COMB3) [38], which is an improved version of the original Cu-O COMB2 potential [39], with a charge equilibration method [40,41] being run every 50 time steps to update the atomic charges. We used a timestep Δt=0.5 fs. To emulate the pressure-free surface conditions in a nanowire, we ran all our simulations within the NPT ensemble, utilizing the Nose-Hoover thermostat, while different barostat settings were used for different simulation phases, the details of which are given in the corresponding section. To avoid thermally induced instabilities in our simulations and focus on the structural dynamics of the CuO crystal under specific mechanical stress, we set a low temperature of 1K in the thermostat.

Acknowledgments

This research was funded by the European Union's Horizon 2020 program, under Grant Agreement No. 856705 (ERA Chair "MATTER"). EB and BP were supported by the Latvian Council of Science project lzp-2022/1-0311. TT was supported by the Estonian Research Council, grant No. SJD61. The institute of Solid State Physics, University of Latvia as the Center of Excellence, has received funding from the European Union's Horizon 2020 Framework Programme H2020-WIDESPREAD-01-2016-2017-TeamingPhase2 under grant agreement No. 739508, project CAMART². The authors are grateful to Krisjanis Smits for his assistance in the acquisition of TEM images.

Supporting Information

Supporting Information is available from the Wiley Online Library or from the author.

References

[1] Levitt A P 1970 *Whisker Technology* (Wiley-Interscience)

[2] Chen Y, An X and Liao X 2017 Mechanical behaviors of nanowires *Appl. Phys. Rev.* **4** 031104

[3] Frankberg E J, Kalikka J, García Ferré F, Joly-Pottuz L, Salminen T, Hintikka J, Hokka M, Koneti S, Douillard T, Le Saint B, Kreiml P, Cordill M J, Epicier T, Stauffer D, Vanazzi M, Roiban L, Akola J, Di Fonzo F, Levänen E and Masenelli-Varlot K 2019 Highly ductile amorphous oxide at room temperature and high strain rate *Science* **366** 864–9

[4] Östlund F, Rzepiejewska-Malyska K, Leifer K, Hale L M, Tang Y, Ballarini R, Gerberich W W and Michler J 2009 Brittle-to-Ductile Transition in Uniaxial Compression of Silicon Pillars at Room Temperature *Adv. Funct. Mater.* **19** 2439–44

[5] Wu Y, Rao Q, Best J P, Mu D, Xu X and Huang H 2022 Superior Room Temperature Compressive Plasticity of Submicron Beta-Phase Gallium Oxide Single Crystals *Adv. Funct. Mater.* **32** 2207960

[6] Mignerot F, Kedjar B, Bahsoun H and Thilly L 2021 Size-induced twinning in InSb semiconductor during room temperature deformation *Sci. Rep.* **11** 19441

[7] Polyakov B, Vlassov S, Dorogin L M, Butikova J, Antsov M, Oras S, Lõhmus R and Kink I 2014 Manipulation of nanoparticles of different shapes inside a scanning electron microscope *Beilstein J. Nanotechnol.* **5** 133–40

[8] Jiang X, Herricks T and Xia Y 2002 CuO Nanowires Can Be Synthesized by Heating Copper Substrates in Air *Nano Lett.* **2** 1333–8

[9] Polyakov B, Dorogin L M, Vlassov S, Antsov M, Kulis P, Kink I and Lohmus R 2012 In situ measurements of ultimate bending strength of CuO and ZnO nanowires *Eur. Phys. J. B* **85** 366

[10] Polyakov B, Vlassov S, Dorogin L M, Kulis P, Kink I and Lohmus R 2012 The effect of substrate roughness on the static friction of CuO nanowires *Surf. Sci.* **606** 1393–9

[11] Sheng H, Zheng H, Cao F, Wu S, Li L, Liu C, Zhao D and Wang J 2015 Anelasticity of twinned CuO nanowires *Nano Res.* **8** 3687–93

[12] Wang R-C, Lin S-N and Liu J 2017 Li/Na-doped CuO nanowires and nanobelts: Enhanced electrical properties and gas detection at room temperature *J. Alloys Compd.* **696** 79–85

[13] Gao W, Yang S, Yang S, Lv L and Du Y 2010 Synthesis and magnetic properties of Mn doped CuO nanowires *Phys. Lett. A* **375** 180–2

[14] Li L, Chen G, Zheng H, Meng W, Jia S, Zhao L, Zhao P, Zhang Y, Huang S, Huang T and Wang J 2021 Room-temperature oxygen vacancy migration induced reversible phase transformation during the anelastic deformation in CuO *Nat. Commun.* **12** 3863

[15] Uttam P, Kumar V, Kim K-H and Deep A 2020 Nanotwinning: Generation, properties, and application *Mater. Des.* **192** 108752

[16] Vlassov S, Oras S, Polyakov B, Butanovs E, Kyritsakis A and Zadin V 2022 Kinking in Semiconductor Nanowires: A Review *Cryst. Growth Des.* **22** 871–92

[17] Tian B, Xie P, Kempa T J, Bell D C and Lieber C M 2009 Single crystalline kinked semiconductor nanowire superstructures *Nat. Nanotechnol.* **4** 824–9

[18] Jiang Z, Qing Q, Xie P, Gao R and Lieber C M 2012 Kinked p–n Junction Nanowire Probes for High Spatial Resolution Sensing and Intracellular Recording *Nano Lett.* **12** 1711–6

[19] Gan L, Liao M, Li H, Ma Y and Zhai T 2015 Geometry-induced high performance ultraviolet photodetectors in kinked SnO2 nanowires *J. Mater. Chem. C* **3** 8300–6

[20] Jiang J-W and Rabczuk T 2013 Mechanical oscillation of kinked silicon nanowires: A natural nanoscale spring *Appl. Phys. Lett.* **102** 123104

[21] Jiang J-W, Zhao J-H and Rabczuk T 2013 Size-sensitive Young's modulus of kinked silicon nanowires *Nanotechnology* **24** 185702

[22] Jing Y, Zhang C, Liu Y, Guo L and Meng Q 2015 Mechanical properties of kinked silicon nanowires *Phys. B Condens. Matter* **462** 59–63

[23] Dorogov M, Kalmykov A, Sorokin L, Kozlov A, Myasoedov A, Kirilenko D, Chirkunova N, Priezzheva A, Romanov A and Aifantis E C 2018 CuO nanowhiskers: preparation, structure features, properties, and applications *Mater. Sci. Technol.* **34** 2126–35

[24] Polyakov B, Kuzmin A, Vlassov S, Butanovs E, Zideluns J, Butikova J, Kalendarev R and Zubkins M 2017 A comparative study of heterostructured CuO/CuWO4 nanowires and thin films *J. Cryst. Growth* **480** 78–84

[25] Yamada H, Zheng X-G, Soejima Y and Kawaminami M 2004 Lattice distortion and magnetolattice coupling in CuO *Phys. Rev. B* **69** 104104

[26] Christian J W and Mahajan S 1995 Deformation twinning *Prog. Mater. Sci.* **39** 1–157

[27] Bao P, Wang Y, Cui X, Gao Q, Yen H-W, Liu H, Kong Yeoh W, Liao X, Du S, Hoe Tan H, Jagadish C, Zou J, Ringer S P and Zheng R 2014 Atomic-scale observation of parallel development of super elasticity and reversible plasticity in GaAs nanowires *Appl. Phys. Lett.* **104** 021904

[28] Yin S, Cheng G, Richter G, Gao H and Zhu Y 2019 Transition of Deformation Mechanisms in Single-Crystalline Metallic Nanowires *ACS Nano* **13** 9082–90

[29] Roos B, Kapelle B, Richter G and Volkert C A 2014 Surface dislocation nucleation controlled deformation of Au nanowires *Appl. Phys. Lett.* **105** 201908

[30] Kim S-H, Kim H-K, Seo J-H, Whang D-M, Ahn J-P and Lee J-C 2018 Deformation twinning of ultrahigh strength aluminum nanowire *Acta Mater.* **160** 14–21

[31] Vlassov S, Mets M, Polyakov B, Bian J, Dorogin L and Zadin V 2019 Abrupt elastic-to-plastic transition in pentagonal nanowires under bending *Beilstein J. Nanotechnol.* **10** 2468–76

[32] Zhu Y T, Liao X Z and Wu X L 2012 Deformation twinning in nanocrystalline materials *Prog. Mater. Sci.* **57** 1–62

[33] Seo J-H, Yoo Y, Park N-Y, Yoon S-W, Lee H, Han S, Lee S-W, Seong T-Y, Lee S-C, Lee K-B, Cha P-R, Park H S, Kim B and Ahn J-P 2011 Superplastic Deformation of Defect-Free Au Nanowires via Coherent Twin Propagation *Nano Lett.* **11** 3499–502

[34] Antsov M, Polyakov B, Zadin V, Mets M, Oras S, Vahtrus M, Lõhmus R, Dorogin L and Vlassov S 2019 Mechanical characterisation of pentagonal gold nanowires in three different test configurations: A comparative study *Micron* **124** 102686

[35] Klinger M 2017 More features, more tools, more CrysTBox *J. Appl. Crystallogr.* **50** 1226–34

[36] Plimpton S 1995 Fast Parallel Algorithms for Short-Range Molecular Dynamics *J. Comput. Phys.* **117** 1–19

[37] Thompson A P, Aktulga H M, Berger R, Bolintineanu D S, Brown W M, Crozier P S, in 't Veld P J, Kohlmeyer A, Moore S G, Nguyen T D, Shan R, Stevens M J, Tranchida J, Trott C and Plimpton S J 2022 LAMMPS - a flexible simulation tool for particle-based materials modeling at the atomic, meso, and continuum scales *Comput. Phys. Commun.* **271** 108171

[38] Liang T, Shan T-R, Cheng Y-T, Devine B D, Noordhoek M, Li Y, Lu Z, Phillpot S R and Sinnott S B 2013 Classical atomistic simulations of surfaces and heterogeneous interfaces with the charge-optimized many body (COMB) potentials *Mater. Sci. Eng. R Rep.* **74** 255–79

[39] Devine B, Shan T-R, Cheng Y-T, McGaughey A J, Lee M, Phillpot S R, Sinnott S B, and others 2011 Atomistic simulations of copper oxidation and Cu/Cu 2 O interfaces using charge-optimized many-body potentials *Phys. Rev. B* **84** 125308

[40] Rappe A K and Goddard W A I 1991 Charge equilibration for molecular dynamics simulations *J. Phys. Chem.* **95** 3358–63

[41] Rick S W, Stuart S J and Berne B J 1994 Dynamical fluctuating charge force fields: Application to liquid water *J. Chem. Phys.* **101** 6141–56